Silver nanowire networks coated with a few nanometer thick aluminum nitride films for ultra-transparent and robust heating applications

Dorina Papanastasiou, Arnaud Mantoux, Alexandre Crisci, Hugo Ribeiro, Abderrahime Sekkat, Hervé Roussel, Matthieu Weber, Laetitia Rapenne, Carmen Jiménez, Marc Fivel, et al.

Silver Nanowire Networks coated with a few nanometer thick Aluminium Nitride Films for Ultra-Transparent and Robust Heating Applications.

Dorina T. Papanastasiou[a,b], Arnaud Mantoux[c], Alexandre Crisci[c], Hugo Ribeiro[c], Abderrahime Sekkat[a,d], Hervé Roussel[a], Matthieu Weber[a], Laetitia Rapenne[a], Carmen Jiménez[a], Marc Fivel[c], Daniel Bellet[a], Elisabeth Blanquet[c,], David Muñoz-Rojas[a,*].*

[a]Univ. Grenoble Alpes, Grenoble INP, LMGP, CNRS UMR 5628, F-38016 Grenoble, France

[b]The University of Tokyo, LIMMS, CNRS-IIS IRL 2820, Tokyo 153-8505, Japan

[c]Univ. Grenoble Alpes, Grenoble INP, SIMaP, CNRS UMR 5266, F-38000 Grenoble, France

[d]Laboratoire de Génie Chimique, Université de Toulouse, CNRS, INPT, UPS, F-31432, Toulouse, France

KEYWORDS: nanocomposites, stability enhancement, atomic layer deposition, metal nitride thin films, scratch tests, transparent heaters

ABSTRACT Transparent electrodes based on emerging nanomaterials like silver nanowire (AgNW) networks have been extensively investigated in the last few years. Thanks to their superior flexibility and versatility in terms of fabrication and device integration, they present an excellent alternative to indium tin oxide. However, the lack of thermal, electrical, and chemical stability requires the encapsulation of the AgNW. This has been done using thin metal oxide films, graphene, or organic protective coatings. Despite the very promising properties of such nanocomposite approaches and the performance enhancement, more investigation is needed to minimize the loss of optical transmittance upon coating and to achieve superior electrical, thermal, and mechanical stability. In the present work, the encapsulation of AgNW networks with aluminium nitride (AlN) coatings is reported for the first time, and it is compared to AgNW/Al_2O_3 nanocomposites. Thanks to the low thicknesses (<20 nm) and the wide bandgap of AlN, the optical transparency is not impacted. Furthermore, the nanocomposite networks demonstrate no failure under electrical and thermal stress conditions (up to 21 V and 400 °C respectively), in contrast to the AgNW/Al_2O_3 nanocomposites, which fail after 15 V and 350 °C. In addition, micro-scratch tests revealed the remarkable mechanical robustness of the nanocomposites, and the electrical stability was further confirmed under accelerated environmental tests, coupled with *ex situ* characterisation by SEM and XPS. The results reported in the present work show that AgNW/AlN electrodes are outstanding candidates for high-performance transparent electrodes.

TEXT

1. Introduction

Over the past decade, research of emerging transparent conductive materials (TCM) has grown exponentially, thanks to their remarkable properties and the exciting opportunities they can provide to a large variety of devices, i.e., touch screens, smart windows, organic photovoltaics, energy harvesters, transparent heaters (TH) or biomedical sensors.[1–3] In the race to replace Indium Tin Oxide (ITO), which is limited by film brittleness and scarcity of Indium, metallic nanowire networks and grids, graphene-based thin films, conductive polymers, and several composite materials have demonstrated excellent electrical, optical, and mechanical properties.[1,4–6] Among them, AgNW networks are one of the most promising alternatives since they can be fabricated in open-air and using large-scale deposition processes, and they have superior flexibility compared to ceramic transparent conductive oxides (TCO).[7–10] However, there are crucial stability issues (chemical, thermal, and electrical) that have hindered their mass integration in devices.[11–13] A common strategy to improve the stability of AgNW networks has been to their encapsulation with a protective layer (typically metal oxides, graphene oxide, or polymer-based thin films) to prevent chemical reactions with the environment and silver atomic diffusion.[6,14–16] Despite the very promising results achieved so far thanks to such protective layers, there is still much room to

improve the voltage and/or temperature of failure and to overcome limitations regarding the loss of optical transparency and long-term stability.[12,14,17,18]

It is thus worth exploring other materials to encapsulate AgNW networks. In this context, Patil et al. recently introduced the use of oxynitrides as protective coating. Namely, oxynitrides of Al, Ti, and Zr (AlO_xN_y, TiO_xN_y, ZrO_xN_y) were deposited by sputtering, leading to the enhancement of thermal, electrical, and chemical stability of the networks.[19] However, for the case of AlO_xN_y, which demonstrated the best performance, the stability enhancement obtained was comparable to the ones obtained with metal oxides.[1,20] While such results are promising, the use of pure nitrides to protect AgNW networks is still unexplored. A recent work presents the deposition of Boron nitride (BN) on copper nanowires (CuNW) by CVD.[21] While the results are again very appealing, showing a strong enhancement of the stability of the CuNW networks, the electrical resistance of the resulting nanocomposites increased largely (60 Ω/sq) for the more transparent networks (>90%) and the high temperatures required to fabricate the nanocomposite (800 ˚C) make the process not suitable for soft substrates and mass production.

Metal nitrides represent an appealing alternative stable and robust coating, with a wide range of physical properties and complementary advantages to oxides, offering a high degree of flexibility

when designing a TE for specific applications. For instance: aluminium nitride (AlN) is a multifunctional material that has been widely studied for many potential applications in recent years, due to its high melting point, very good chemical stability and excellent thermal conductivity compared to other nitrides or oxides.[22] In addition, it is self-protecting in oxidizing environments, because it shows a low oxidation rate even at high temperatures up to 1100 ˚C (thanks to the formation of a passivating Al_2O_3 layer). Thus, it has a broad range of applications in micro- and nano- scale optoelectronic devices, including dielectric and passivation layers, but also electrothermal film heaters.[23–26] Finally, AlN has a wide band gap leading to transparency even in the UV region, which makes it very promising for applications such as transparent heaters or electrodes for windows and UV applications. Moreover, metal nitrides can be easily deposited in a very conformal way, with a highly precise control of the thickness, and at low temperatures via atomic layer deposition (ALD), including the more recent Atmospheric Pressure-Spatial ALD (AP-SALD) approach that is faster and more suitable for low-cost mass production.[27,28]

The present study reports, for the first time, the development of a nanocomposite transparent electrode based on AgNW networks and pure AlN thin film coatings. Various thicknesses of AlN coatings have been investigated, deposited by plasma-enhanced ALD (PE-ALD), at rather mild

temperatures (250 ˚C). The optical, chemical, electrical, and mechanical properties and stability have been evaluated, including *in situ* measurements of electrical resistance and spatial distribution of temperature by IR imaging. Ultra-thin AlN (<20 nm) yield highly transparent (~85%) and conductive (10-15 Ω/sq) networks with an outstanding stability which has not been reported by other protective coatings so far: no failure occurred under thermal stress (temperature reaching 400 ˚C), electrical stress (over 20 V), even after several testing cycles. In addition, AlN coatings provide a successful barrier against humidity (RH-80%, Temp-70 ˚C). A high adhesion and a remarkable mechanical stability of the nanocomposite electrodes have been confirmed by subjecting them to an alcohol-immersed ultrasonic bath test and to micro scratch tests. The latter has not been widely used for the characterization of AgNW networks and their nanocomposites so far. Another important feature of the present work is the use of several techniques, like XPS and SEM, to evaluate *ex situ* the efficiency of AlN, and reveal effects that are invisible during electrical tests. Finally, the comparison with aluminium oxide Al_2O_3 thin films with similar thicknesses deposited by AP-SALD has demonstrated that nitride coatings are still the most efficient strategy. All in all, the present results of AgNW/AlN nanocomposites pave the way for the development of

high performance, robust transparent electrodes and heaters, and their integration into a large variety of devices.

2. Results & Discussion

2.1 Fabrication of AgNW/AlN nanocomposites and main properties

AgNW networks were deposited by spray coating on glass substrates with targeted electrical resistance around 15 Ω sq^{-1} and optical transparency of ≈85% (including substrate contribution), as in our previous reports.[13,29] The surface area coverage of the AgNW networks is 13 ± 2 % and in terms of the amount of silver, the areal mass density (*amd*) is 70 ± 5 mg m^{-2}, taking into account the dimensions of the nanowires in the estimation.[20] AlN thin coatings were directly deposited on top of the AgNW networks by plasma-enhanced atomic layer deposition, as previously reported by Tian et al.,[23] at 250 ˚C. Such value is below the degradation temperature of the AgNW networks as well.[20] A schematic representation of PE-ALD is presented in **Figure 1a**, as well as the process of metal oxide coatings by AP-SALD in **Figure 1b**, which are compared in the last part of this study. Full details of the materials and the deposition techniques are reported in the Materials and Methods section, as well as all the characteristics of the instrumentation used for the evaluation of

the transparent electrodes. The thickness of the AlN coating was varied to investigate its influence on the stability of the AgNW networks during electrical, thermal, mechanical, and environmental tests, presented in the following sections of the article. Four different AlN thicknesses were chosen, between 5 and 20 nm, and for each AlN thickness, three different AgNW/AlN were fabricated, to evaluate the electrical and optical properties reproducibility and the stability under several tests. **Figures 1c** and **d** show the morphological characteristics of bare and AlN coated AgNW networks. Due to the small thickness of AlN coatings, even for the thickest case, it is challenging to distinguish the coatings by SEM. However, the images show that the coating is very conformal. This was indeed validated by TEM, as shown in **Figure 1e** and **f**. From the TEM observations, the film thickness on Ag nanowires is 5 nm and 12 nm for the thinnest and for intermediate thickness films, respectively. The TEM image in **Figure S1**a illustrates the monocrystalline nature of AgNW, showcasing distinct planes,[30] while revealing the amorphous structure of the AlN layer. For a better estimation of the thickness of the AlN coating, X-ray reflectivity (XRR) was also used on AlN coatings deposited on glass using the same conditions and number of ALD cycles as for the coating the wires. (see **Figure S2** in Supporting Information). For the thinner AlN coating on glass, the thickness obtained was 6.2 ± 0.2 nm (instead of 5 nm on AgNW-Figure 1), while for the thicker

one it was 19.6 ± 0.2 nm (instead of 12 nm on AgNW), i.e., an average growth per cycle (GPC) of 0.05 nm/cycle. It should be noticed at this point that the GPC on glass and AgNW does not follow an ideal ALD evolution, as expected at this growth temperature outside the ALD window as previously evaluated on silicon substrates.[23] However, the average estimated GPC is in the same order of magnitude as that obtained on silicon.

The optical and electrical properties were measured on each sample both before and after AlN deposition and the mean values for each UV, Visible and NIR spectra, at each AlN thickness were calculated, to study precisely the influence of the AlN coating and provide a fair comparison between bare samples and nanocomposites (see details about the method followed in Materials & Methods). The full spectra of the total transmittance of bare and coated AgNW networks are presented in **Figure 1g**. The values of Corning glass substrate are presented as a reference (in black dashed line). The AgNW/AlN nanocomposites are referred to by a "C" (coated), followed by the value of the corresponding AlN coating thickness on glass (in nm). This description is consistently followed to the rest of the manuscript. Finally, the mean values obtained are shown in the inset of Figure 1g (mean value difference at each spectrum, for each coating thickness). The results show only a minor influence of the AlN coating in the optical properties of the electrodes, which can be

attributed to the high optical transparency of bare AlN coatings, confirmed in the present work (Figure S1b). The optical band gap of bare AlN coatings is calculated by Tauc plot (inset of Figure S1b), showing values between 3.45 and 3.5 eV. For the AgNW/AlN nanocomposites, the statistical estimation in the inset of Figure 1g shows that indeed, in the UV and Visible range, the transmittance only slightly decreases as the AlN coating thickness increases (-2.4 ± 0.2) %. In the NIR range, the optical properties are not only sustained, but there is a slight increase of the optical transparency, up to 0.4%. Such values show that, compared to other protective coatings, the high transparency of the AlN, make it an excellent choice for the AgNW networks.[12,14] A photo of the AgNW/AlN highlighting the high optical transparency of the nanocomposite is presented in Figure S1c.

The electrical properties of the AgNW/AlN nanocomposites, along with the total transmittance for each nanocomposite at 550 nm, are presented in the box chart of Figure S1d. The discrepancy in the values of electrical resistance is attributed to statistical variation of the spray coating technique (see Materials & Methods). The insulating nature of as-deposited AlN coatings was confirmed by four-probe measurements that demonstrated values in the range of 500 MΩ - 1 GΩ. In addition, the Figure of Merit (FoM) of the AgNW/AlN nanocomposites was calculated, with

the maximum value being 13.4 x10^{-3} Ω^{-1} and the mean value being 9.6 ± 2 .0 x10^{-3} Ω^{-1} (the glass substrate is included in the calculations). Such values are within the target performance of transparent electrodes, and they could be further improved by tuning the AgNW dimensions (i.e., longer nanowires).[1]

The chemical composition of the AgNW/AlN nanocomposites was investigated by XPS, **Figure 1h**, for bare and coated AgNW networks. The characteristic Ag peaks that appear as expected at 368 eV and 374 eV for bare AgNW network, disappeared in the case of AgNW/AlN nanocomposite, meaning that the network was successfully covered by the PE-ALD process. The other elements spectra (Al2p, N1s, O1s, C1s) for AgNW/AlN are presented in **Figure S3**. The peak in Al2p is the signature of the AlN bond,[31] and the peak in N1s, which corresponds to N bonded to the metal in AlN, illustrate the fact that a pure nitride material has been obtained as previously reported.[32] The peak related to the C-C bond in C1s is due to the surface contamination. Following the elaboration of AgNW/AlN transparent electrodes and the evaluation of their main properties, the stability performance during several types of stress is presented and discussed in the next sections.

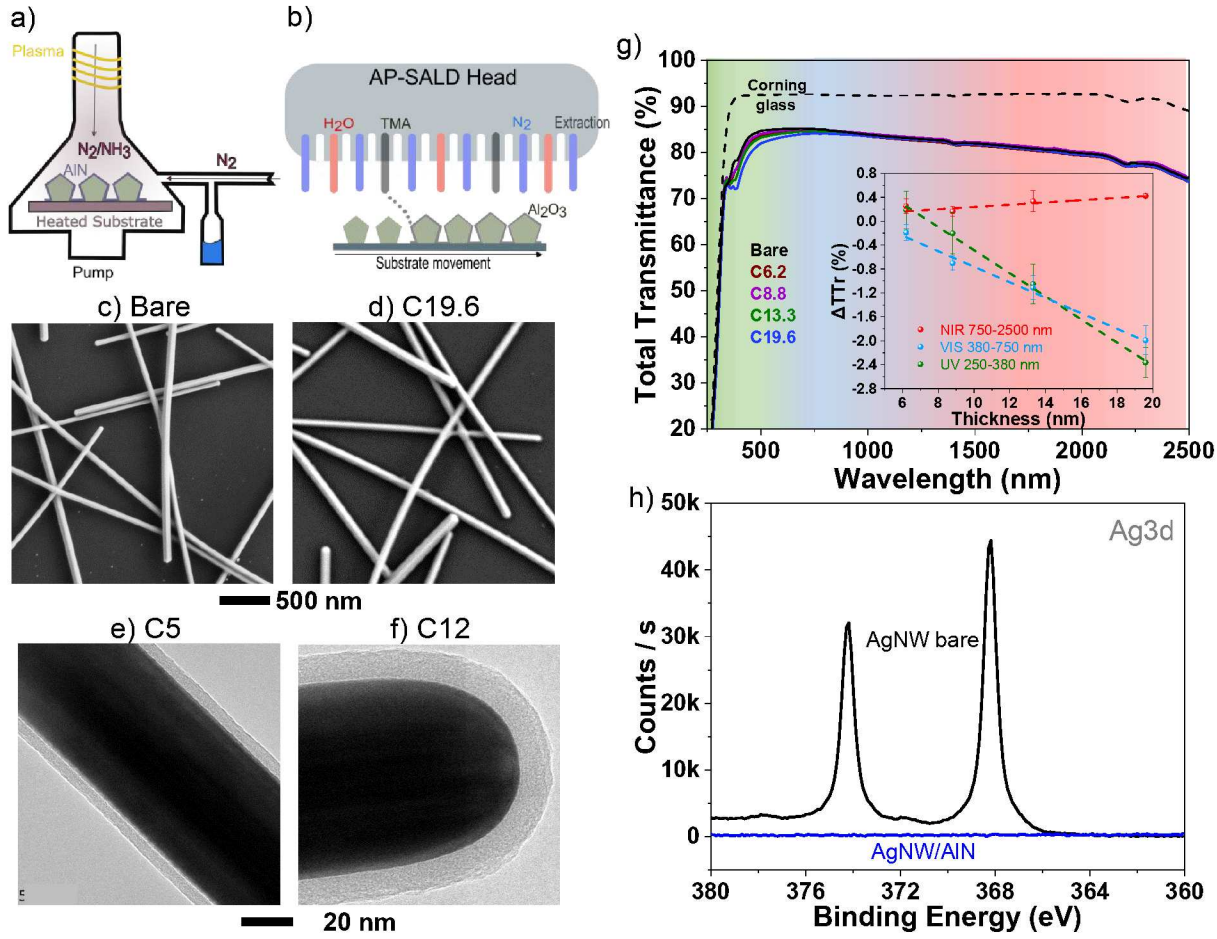

Figure 1: a-b) Schematic representation of the processes to coat the AgNW networks: AlN by PE-ALD and Al_2O_3 by SALD, respectively. c-f) SEM and TEM of AgNW bare and AgNW/AlN nanocomposites of several thicknesses. g) Total Transmittance in UV-VIS-NIR range and mean values of difference in transmittance before and after coating, calculated for each range. h) XPS spectra of the Ag3d region of bare and AlN thicker coating, C19.6 nm, on top of AgNW network.

2.2 Electrical stability during accelerated environmental stress and mechanical durability

First, an accelerated environmental stress test was performed. A bare AgNW network and the four AgNW/AlN nanocomposites with varying thickness were placed inside an environmental

chamber with 70 ˚C temperature and 80% relative humidity for 9 days. The evolution of the normalized electrical resistance (measured resistance R versus the initial resistance R_o), shown in **Figure 2a**, clearly demonstrates the superior stability of the nanocomposites thanks to the thin AlN coatings. The electrical resistance of the bare network started to increase during the very first hours and diverged completely during the third day of the experiment, while the resistance of the nanocomposites stayed stable for the whole nine days of the experiment. The inset in Figure 2a is a zoom during the last day, showing almost zero increase of resistance. The absolute values before and after the experiment are shown in **Table S1**. Furthermore, XPS was performed to investigate the impact of accelerated environmental stress (**Figure S4**). Interestingly, Ag peaks could be detected for AgNW/AlN sample after the experiment, but at a lower intensity compared to the as-deposited bare AgNW. Considering the high stability related to the electrical resistance, this result can be the sign of a possible local degradation of the prepared layer, that led to the migration of Ag out of the coating. This feature will be discussed in the following experiments as well. Furthermore, the samples were subjected to an ultrasonic bath in IPA for 15 minutes, while the electrical resistance was measured continuously *in situ*. The bare AgNW and the thicker AlN nanocomposite (19.6 nm) were chosen, and the evolution of the electrical resistance are shown in

Figure 2b. Again, the bare AgNW network starts to degrade fast, while the AlN coating seems to offer superior protection against the mechanical stress induced by the ultrasonic bath.

The next method that was chosen to access the mechanical resistance of bare AgNW and their AlN nanocomposites was the micro-scratch tests. Previously nano-indentation has been used to measure the hardness and elastic modulus of a single Ag nanowire compared to bulk Ag or studies of plastic deformation, always at the nanoscale.[33,34] However, to the best of our knowledge, the efficacy of coatings on AgNW networks hasn't been assessed using the micro-scratch test method. Such tests involve applying a constant or increasing load on an indenter moving at a fixed velocity. In the present work, 4 mm long linear scratches with a 100 μm radius diamond spherical tip were performed into bare AgNW and AlN nanocomposites of different thicknesses. Then, SEM imaging was used to reveal the impact of such load at the microscale with constant or increasing force from 10 mN up to 30 N. In the case of bare AgNW, as the SEM images show in **Figure 2c** and **d**, the nanowires were completely removed at 10 mN; the lowest possible load of the set-up. In the case of AlN nanocomposites, the thinner AlN coating (6.2 nm) was not enough to protect them either, whereas the coatings with thicknesses of 8.8, 13.3 and 19.6 nm proved to be very robust. Not only did the AgNW sustain much higher loads, but they also showed an excellent adhesion to the glass

substrate, even when subjected to loads that lead to the local fracture of the glass substrate. Such results can be observed in the SEM image in **Figure 2e** after the application of 15 N force on AgNW/AlN-8.8 nm, where the AgNW were squeezed but not removed (conversely to the bare network), and after an increasing force up to 30 N (**Figure 2f**), where surprisingly the AgNW/AlN remained attached to the substrate in the tiny pieces of the broken glass after the indenter passage. The visible splinters may have detached ahead of the tip when the substrate started to break. Further SEM images, for several AlN thicknesses, are provided in **Figure S5**.

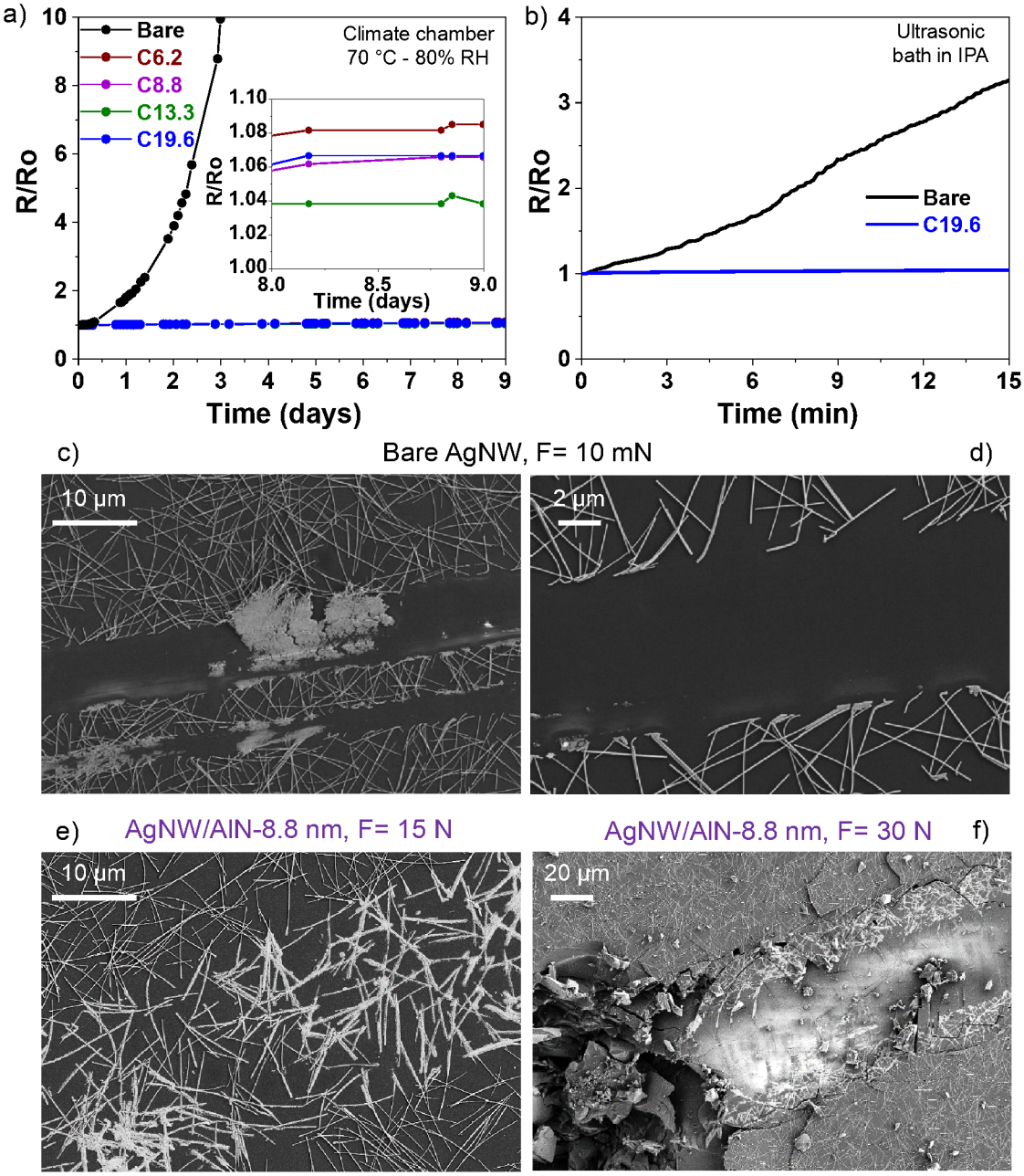

Figure 2: Normalized electrical resistance evolution for bare and AlN coated AgNW networks, measured during a) environmental stress inside a climate chamber of 70 ˚C temperature and 80% relative humidity for 9 days, and b) ultrasonic chemical bath in IPA. c-d) SEM images of bare AgNW network after a scratch performed with a constant normal force of 10 mN. e) AlN 8.8 nm coated AgNW network at 15 N normal force and f) AlN 8.8 nm coated AgNW network at the maximum force of 30 N.

2.3 Electrical stability enhancement of AgNW network during electrical and thermal stress with AlN coatings

In this section, the stability enhancement during electrical and thermal stress tests (increasing ramp and repeated cycles) is discussed. Several thicknesses of AlN coatings were investigated, offering drastic stability enhancement. For the sake of simplicity, only the thicker AlN case (19.6 nm) is presented in **Figure 3**. This is the thickness that showed the best protection during the above mechanical tests as well. The performance of the rest of thicknesses will be provided in the last section, when compared to nanocomposites made with Al_2O_3 coatings of similar thickness. The first electrical test includes the application of a constantly increasing voltage (0.5 V/min ramp), with the simultaneous recording of the electrical resistance and the spatial distribution of surface temperature (Joule effect by IR imaging). The normalized electrical resistance evolution is presented in Figure 3a, with initial values being 19 Ω and 18 Ω, for bare and nanocomposite networks, respectively. As it was expected and reported in several previous studies,[20,35,36] the electrical resistance of the AgNW started to increase after 11 V and completely degraded before reaching 13 V. However, in the case of the nanocomposites with AlN, the samples show full

stability until more than 20 V. It should be noted that the measurement was automatically stopped at 21 V as the current compliance of the instrument was reached. Furthermore, the inset of Figure 3a are IR images at the moment of failure of bare AgNW and at the maximum applied voltage (21 V) for the AgNW/AlN nanocomposite. For the bare case this signifies the propagation of the hotspot as it has been studied previously.[37] In the case of the nanocomposite, a homogeneous distribution of the surface temperature can be observed as well as high achieved temperatures. Such performance can be also attributed to the high thermal conductivity of AlN and the efficient heat spreading, as it has been reported for the case of thin films or inks.[25,38] Additional videos of the *in situ* IR imaging can be found in SI (Movies S1-S2). After the voltage ramp, the samples were subjected to continuous electrical stress, at voltage plateaus of 8 and 11 V (below the bare AgNW failure voltage), each for 5 min. Figure 3b presents the relative variation of electrical resistance versus time; the initial resistance values being 13 Ω and 15 Ω, for bare and AlN coated AgNW networks, respectively. The bare network showed an irreversible increase in the electrical resistance after 7 voltage cycles, while the AlN coated samples showed a stable electrical response for more than 4.5 hours. It is important to note that the AgNW/AlN nanocomposite had been subjected to the previous voltage ramp, before undergoing the additional voltage cycles stress. In

conclusion, the AlN coatings improve drastically the electrical resistance and it is, to the best of our knowledge, the most successful thin film coating to protect AgNW networks reported so far.[12,14] Such results can be useful for transparent heater applications with superior stability and heating efficiency.

Regarding the stability of the transparent electrodes under thermal stress, similarly, a thermal ramp was applied at first, to investigate the temperature of degradation and then, thermal cycles were applied continuously. The electrical resistance was measured *in situ* during the thermal annealing (all details in Materials & Methods). Figure 3c presents the relative resistance variation versus the applied temperature, during the thermal ramp of 5 ˚C/min until 400 ˚C and back to room temperature with the same ramp. After 300 ˚C, the bare AgNW network demonstrated an irreversible resistance increase, due to the spheroidization of the nanowires and the destruction of percolation pathways.[6] Conversely, the AgNW/AlN nanocomposites demonstrated again a fully stable performance, showing no degradation; actually, the resistance even decreased slightly (from 24.5 to 23 Ω). An additional comment about the different response before degradation (225 to 275 ˚C) should be given: the resistance of the AgNW network shows a decrease, which is related to the sintering of the nanowires' junctions thanks to thermal annealing. This optimization process

leads to the decrease of the junctions contact resistance and consecutively, the macroscopic resistance of the network.[13,20] Such phenomena is not presented for the case of AgNW/AlN nanocomposites, probably because the sintering had taken place during the deposition of the AlN by PE-ALD at similar temperature, 250 ˚C. In addition, the presence of plasma could further improve the junctions between the nanowires.[39,40] Another stability test related to thermal stress is the continuous heating cycles between 150 and 300 ˚C (below bare AgNW degradation), with a ramp of ±10 ˚C/min. As presented in Figure 3d, the AgNW/AlN nanocomposite showed excellent stability compared to the bare network, which showed a rapid and irreversible increase from the first cycles. Like the electrical stress tests, the AgNW/AlN nanocomposite has been subjected to the thermal ramp until 400 ˚C before the thermal cycles, but this did not influence its stable performance.

SEM images reveal the morphology of the transparent electrodes after the thermal ramp (Figure 3c inset): the spheroidized bare network versus the AgNW/AlN nanocomposite that does not show any evidence of degradation (additional SEM of the nanocomposite is included in **Figure S6**a). To verify this, we performed XPS survey after the thermal ramp, as it was performed after the accelerated environmental test (see section 2.2). It should be noted that in order not to influence

the XPS signal by the silver paste, the side contacts were deposited after the XPS, to make the resistance measurement. The AgNW/AlN after thermal ramp had the same spectra as the AgNW/AlN as-deposited case; absence of Ag characteristic peaks in the Ag3d (Figure S6c), confirming that the coating was still efficiently protecting the nanowires, leaving no space for Ag diffusion. To investigate the stability under harsher conditions, we performed constant heating at 400 ˚C for 9 hours. The electrical resistance after such condition was still very low, as it is presented in **Table S2**, which includes the electrical resistance of AgNW/AlN as-deposited and after thermal ramp as well. Such resistance value does not indicate any degradation; however, the morphology of the nanocomposite was different this time; nanoparticles have appeared between the (intact) nanowires (SEM images in Figure S6b). The XPS spectra of AgNW/AlN after 9 hours at 400 ˚C was different as well compared to the AgNW/AlN as deposited and AgNW/AlN after thermal ramp. The characteristic peaks of Ag appeared (Figure S6c) with an intensity similar to bare AgNW after thermal ramp, and both higher intensity than the bare AgNW as-deposited. The XPS indicates that the nanoparticles observed in the SEM are result of Ag migration after 9 hours at 400 ˚C. Thus, even if the nanocomposites developed in this work present superior stability than previously reported nanocomposites, a slight degradation under harsh conditions still takes place

and can affect the performance of device in the long-term. As expected, a minor surface oxidation of the nitride layer takes place, as indicated by the slight shift of the peak showed in the Al2p spectrum (Figure S6d). The slight degradation of the networks revealed by XPS is not detectable by the measurement of the electrical resistance, which is the usual evaluation technique presented in literature. Given this, we highlight the need to use several techniques (XPS, SEM, among others) to investigate in a complete way the stability of nanocomposites that combine materials of different nature (thin films and nanomaterials). In conclusion, thanks to the above results the AgNW/AlN nanocomposites are expected to be very stable at the milder conditions used in real applications of transparent heaters.

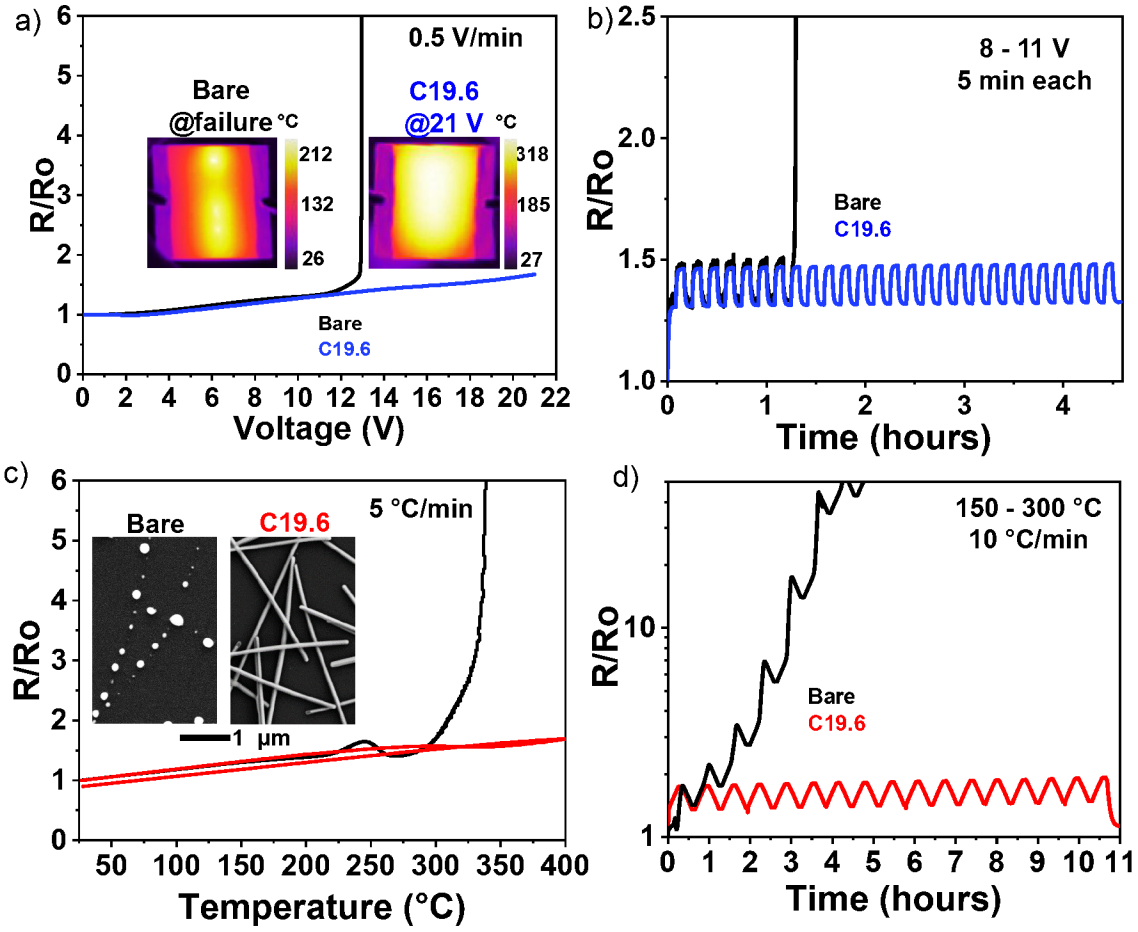

Figure 3: Normalized electrical resistance evolution for AgNW bare (in black) and network coated with 19.6 nm AlN (blue for electrical stress, red for thermal stress), measured *in situ* during: a) voltage ramp 0.5 V/min up to 21 V. Inset IR images demonstrating the failure of bare AgNW network and the Joule heating performance at high voltages for the AlN coated network. b) voltage cycles between 8 and 11 V with 5 min at each plateau. c) thermal ramp up to 400 ˚C and back to room temperature with 5 ˚C/min. Inset SEM images showing the spheroidization of bare AgNW and the stability of AlN coated networks. d) thermal cycles between 150 ˚C and 300 ˚C, with ramps of ±10 ˚C/min and 5 min at each plateau.

2.4 Comparison between Nitride vs Oxide coatings of similar thicknesses

In the last part of the study, the AgNW networks stability enhancement by AlN is compared with the protection conferred by Al_2O_3 thin film coatings of similar thickness, deposited by spatial atomic layer deposition (all details in Materials & Methods section). TEM imaging demonstrated a quite conformal coating around the nanowires (**Figure S7**a). The color code followed in this part to distinguish the coatings is purple shades for the nitride and green shades for the oxide ones. The optical properties of AgNW/Al_2O_3 nanocomposites are presented in Figure S7b, in comparison to the AgNW/AlN of similar coating thicknesses, and full details of electrical and optical properties are provided in **Table S3**. The electrical resistance was noticeably influenced by the Al_2O_3, after the deposition of the thicker coating (13.0 nm). The calculations and comparison of optical transmittance before and after oxide coating was done as described in the Materials and Methods section. As it is shown in Figure S7b, the decrease is similar for the oxide and the nitride coatings, as expected given that they presented similar band gaps (3.65 eV calculated for Al_2O_3, see Supporting Information, Fig. S1b and S7c). The thickness of the coatings affects the transparency of the composites as expected, but even with the thickest coatings, transparency losses do not exceed 3%. In the NIR range, the Al_2O_3 coated AgNW networks become more transparent as previously reported.[41] Finally, the FoM for AgNW/Al_2O_3 transparent electrodes has a maximum

value of 10.8×10^{-3} Ω^{-1} and mean value $8.0 \pm 2.7 \times 10^{-3}$ Ω^{-1} (glass substrate included), which are both a little lower than those of AgNW/AlN (section 2.1).

Concerning the stability enhancement comparison, a voltage ramp up to 20 V (0.5 V/min) and then a thermal ramp up to 400 ˚C (5 ˚C/min) were applied, and the electrical performance of the nitride and oxide-based nanocomposites is presented in **Figure 4**. This figure also provides all the results related to the AlN nanocomposites of different thicknesses, as it was mentioned in section 2.3. From a first overview, it is obvious that the Al_2O_3 enhances the stability of bare AgNW networks, but still the oxide-based nanocomposites fail at higher applied voltage or temperature, while the nitride-based are very stable. More specifically, the AgNW/Al_2O_3 nanocomposites reach a failure voltage around 15 V (Figure 4a), higher than the bare case. Only the thicker Al_2O_3 case degrades at a low voltage and seems inefficient for the protection of the AgNW networks. Even though such tendency may appear counterintuitive, it has already been reported and discussed previously in the literature, where an intermediate thickness of AlO_x thin film coating was optimum.[35,41] On the contrary, the nitride coatings are much more robust: only for the AlN-6.2 nm nanocomposite, the electrical resistance increased just before 20 V, while all the rest cases, 8.8 and 13.3 nm never failed, same as the 19.6 nm presented in Figure 3. Additional videos of the *in situ*

IR imaging can be found in SI (Movies S3-S8). Similarly for the thermal stress, the oxide coated networks showed a higher temperature of degradation than the bare AgNW, around 350 ˚C. Indeed, SEM imaging (Figure S8a-d) revealed an obvious, partial degradation of the AgNW/Al_2O_3 nanocomposites after annealing. The oxide coatings failed to fully protect the nanowires at high temperatures. In other recent studies, AlO_x coatings deposited on AgNW networks by ALD or solution based techniques, were integrated successfully as passivation layers against humidity while still degradation occurred at high applied voltages.[35,42] On the contrary, the nitride coated networks demonstrated superior stability until 400 ˚C and once back to room temperature they had the similar or even lower final electrical resistance; for the AlN-6.2 nm the resistance increased 15% while for the AlN-8.8 nm AlN-13.3 nm AlN-19.6 nm the resistance decreased -6.2%, -10.5% and -6.5% after annealing. In conclusion, the encapsulation of AgNW networks is necessary to develop transparent electrodes and the comparison between Al-based nanocomposites, the nitride coatings show a superior efficiency as compared to the oxide coatings.

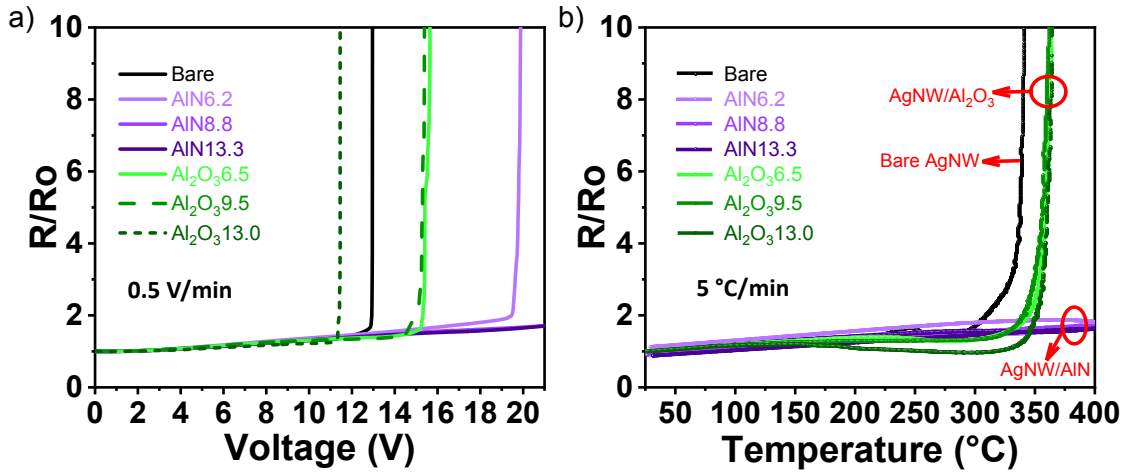

Figure 4: Influence on stability-comparison between bare AgNW (black colour), aluminum oxide (in shades of green) and aluminum nitride (in shades of purple) thin film coatings on top of AgNW networks. a) voltage ramp (0.5 V/min). The Al_2O_3-9.5 nm coating in dashed line and the Al_2O_3-13.0 nm in small-dashed line. The lines of AgNW networks with AlN-8.8 nm and AlN-13.3 nm overlap because these samples remained stable up to 21 V. b) thermal ramp (5 ˚C/min). All AgNW/AlN nanocomposites remain stable up to 400 ˚C (5 ˚C/min), while the resistance of bare AgNW and of all AgNW/Al_2O_3 nanocomposites increases irreversibly.

3. Conclusions

The first AgNW/AlN nanocomposite transparent electrodes were demonstrated in the present work. The nanocomposites where fabricated using scalable and low temperature approaches. Even a low thickness (<20 nm) of nitride coatings, conformally deposited by PE-ALD, was sufficient to enhance drastically the electrical stability of AgNW, as it was demonstrated by several types of stress tests, i.e., environmental, electrical, and thermal. In addition, the AlN coatings provide an

excellent protection without affecting the optical and electrical properties of AgNW networks and micro-scratch tests confirmed the remarkable mechanical robustness thanks to the properties of AlN. Another important aspect of the present study is that mild morphological changes revealed through SEM and XPS, due to Ag diffusion, do not result in an increase of the electrical resistance. This means that electrical/thermal tests alone (*in situ* or *ex situ*) fail to reveal the onset of electrode morphological degradation and therefore cannot be used alone to evaluate the stability of nanocomposite electrodes. Finally, the stability enhancement of nitride-based nanocomposites was compared to that of oxide-based nanocomposites, during electrical and thermal stress. As it has been often observed in the case of oxide protective coatings, the AgNW/Al_2O_3 showed a higher value of voltage or temperature failure (15 V and 350 ˚C) than the bare AgNW (13 V and 325 ˚C). Still, they could not reach the performance of AlN coatings that showed no failure at all (up to 21 V and 400 ˚C). All these results of superior electrical stability, along with the high and homogeneous Joule heating performance, recommend the AgNW/AlN nanocomposites as an outstanding candidate for new generation transparent heaters. Further investigation of the interfaces between AgNW and AlN, as well as the mechanisms responsible for such efficient protection, are of high interest and significance.

4. Materials & Methods

4.1 Materials and deposition techniques

AgNW synthesis and networks fabrication. AgNWs with an aspect ratio close to 100 (average diameter of 70 ± 10 nm and an average length of 8 ± 3 μm) were kindly provided from the research team of Jean-Pierre Simonato from CEA-LITEN in Grenoble, France, being produced as detailed in Mayousse et al.[43] The AgNWs were dispersed in methanol with an initial concentration of 3.1 g/kg and diluted afterwards 30 times to obtain a concentration of 0.1 g/L. Spray deposition was performed with an airbrush of 0.4 mm nozzle size ("Infinity" by Harder & Steenbeck) and a nitrogen inlet of 1.4 bar pressure. The airbrush was fixed in a mechanical setup connected with a programmable automation controller. During deposition, the airbrush was moving along a regular and periodic array in X and Y directions, 7 cm above an aluminium plate set to 110 ˚C, for a direct evaporation of the solvent. The substrates used, Alkaline earth boroaluminosilicate glass (Corning® 1737, thickness 1.1 mm), were cut in squares of 25x25 mm^2, rinsed with acetone, ultrasonicated for 15 min in isopropanol, rinsed with distilled water, and finally dried with N_2 gas.

AlN thin films. AlN thin films were grown by plasma enhanced-atomic layer deposition (PE-ALD) in an ALD R200 Advanced Picosun System reactor, which features Thermal-ALD as well as PE-ALD equipped with an inductively coupled remote plasma (ICP) source. TMA (99.99%, STREM) and NH_3 (99.99%, Air Liquide) were used as Al and N precursors. As detailed in Tian et al.,[23] the pulsing sequence of the PE-ALD of AlN consists of the following steps: (1) TMA pulse, 0.1 s, (2) N_2 purge, 4 s, (3) remote H_2 plasma, 12 s, (4) N_2 purge, 2 s, (5) NH_3 pulse, 5 s and (6) N_2 purge, 4 s. The temperature of the TMA container was kept at 17 ˚C. N_2 was used as carrier gas to transport the TMA and NH_3 precursors to the reactor, with flow rates at 80 and 120 sccm respectively. The plasma power was fixed at 2800 W. Ar was used as a carrier gas for the H_2 plasma (80 sccm) and H_2 flow rate was 100 sccm. The substrate temperature was fixed at 250 ˚C.

Al_2O_3 thin films. Al_2O_3 thin films were deposited by atmospheric-pressure spatial atomic layer deposition (AP-SALD) using a home-made system.[44–46] Trimethylaluminum ($Al(CH_3)_3$; TMA) and water vapor were used as precursors for aluminum and oxygen, respectively. The gas injector was fixed at 150 μm from the substrate, which oscillated at 10 cm/s. The substrate temperature was maintained at 100 ˚C. The TMA was bubbled at 20 sccm and then further diluted with 230

sccm of N_2. H_2O was bubbled with 150 sccm, diluted in 225 sccm of N_2. The N_2 barrier total flow was 750 sccm.

4.2 Experimental characterizations

Surface morphology & chemical composition. AgNW and thin films surface morphology were analyzed by field emission gun-scanning electron microscopy (SEM ZEISS-Gemini 300) and transmission electron microscopy (TEM JEOL JEM-2010 microscope). ImageJ software was used to calculate the AgNW surface area coverage (percentage of white over black pixels on SEM images made binary) as well as the network density, expressed as the areal mass density *amd* (in mg/m^2), by a wire detection plug-in (Ridge detection), estimating the geometrical density in SEM images, following the protocol described somewhere else.[47] For the TEM, the AgNW solution was sprayed directly on Cu-grids placed, followed by the PE-ALD, next to the glass substrates, and the images reveal the high quality of thinner and thicker AlN coatings encapsulating the AgNW. X-ray photoelectron spectroscopy (XPS) measurements were performed using a K-alpha spectrometer from Thermo Fisher Scientific with an Al $K_{\alpha 1,2}$ (1486.6 eV) X-ray source in ultrahigh vacuum (10-8 mbar) at room temperature. The X-Ray beam area (spot size) was adjusted to 400 µm in diameter. To correct for any charging effect, all the binding energies were calibrated to the

C-C component of the C1s core spectrum at 285.0 eV. Core peaks were analyzed using a non-linear Shirley-type background. X-ray reflectivity (XRR) was used to obtain film thickness of AlN coatings, using a Siemens (Bruker) D5000 diffractometer and the data were fitted with Leptos software, using the simulation of one AlN layer on top of SiO_2. Ellipsometry was used to obtain the film thickness of Al_2O_3 coatings, using a compact Film Sense FS-1 ellipsometer.

Electrical & optical properties. The sheet resistance of AlN thin films was measured using a four-probe apparatus (Lucas Labo Pro4), with a device head composed of in-line mounted tungsten probe pins, separated by 1 mm, with a pin radius of 40 μm. To measure the electrical resistance of the bare and coated AgNW networks with two-probe means, silver paste contacts (L-200N purchased from CDS Electronique) were manually deposited at two opposite sides of the samples and dried in room temperature for 1 hour. Optical properties (250–2500 nm range) were investigated in the using a UV/VIS/NIR spectrophotometer equipped with an integration sphere (Lambda 950 Perkin Elmer), using a wavelength step of 10 nm. Then, the mean value for the 3 spectra: i) UV (250-380 nm), ii) Visible (380-750 nm), and iii) NIR (750-2500 nm) was calculated. Also, the mean value difference for each AlN thickness, was also calculated, using 3 samples at each thickness. The great majority of studies provide the difference in respect to a bare AgNW

network as reference. However, even if a spray coating deposition is highly reproducible, a statistical discrepancy between the resulted AgNW networks has been demonstrated, even between those deposited simultaneously.[13,48] The %value of this discrepancy is comparable to the influence of a thin film coating in terms of optical transmittance. Thus, the method followed in the present study allowed to precisely estimate the influence of such coatings to the optical properties of AgNW networks. Also, since the optical properties are directly related to the electrical properties, this process allowed to ensure that the variation of electrical resistance of bare AgNW is very small and the areal mass density is very similar.[13] This is because (apart from the bare ones) the electrical resistance of the samples cannot be measured before the AlN deposition; the silver paste side contacts were deposited after the PE-ALD process and any electrical measurement with two probes before would not have been accurate for the comparison.

Climate chamber, ultrasonic bath, micro-scratch. For the environmental stress, bare AgNW and AlN coated networks were enclosed in an oven (Memmert UN110plus) at 70 ˚C temperature and 80 % relative humidity and their electrical resistance was measured *in situ* every few hours, without opening the chamber door and perturbating these conditions, with a multimeter through long wires stuck to the silver paste electrodes and held outside of the climate chamber. Mechanical durability

tests were conducted with the samples merged inside a beaker filled with isopropanol (IPA) and then placed in an ultrasonic bath cleaner (Elmasonic Elma S15H) with a frequency of 37 kHz. Micro-scratch experiments were performed on a MCT3-Anton PAAR setup, with a diamond Rockwell indenter tip of 100 μm radius mounted in a 120˚ conical tip. For each sample, linear scratches of 4 mm length were performed, either with a constantly increasing or a constant load within the 10 mN-30 N range. The Anton PAAR scratch software gives access to normal force, lateral force, and surface profiles recorded during the execution of the scratch test and synchronized with optical observations.

Electrical & thermal stress, IR imaging. For the electrical and thermal stability tests, the electrical resistance was measured *in situ* through long wires using a Keithley 2400 source-measure-unit (SMU) and recorded by LabVIEW software. For the electrical stability tests, the voltage was applied using the Keithley 2400 SMU, piloted by a LabVIEW program. An IR camera (FLIR T335) was used to evaluate the spatial distribution of the temperature, and the emissivity value used was chosen as 0.9, in accordance to previous reports.[48,49] The electrical stability during thermal stress was investigated by experimental homemade set-up that allows the control of the heating plate temperature (by Eurotherm PLC) and *in situ* recording of the electrical resistance

through a Keithley 2400 SMU while applying a voltage of 100 mV; all this piloted and recorded by LabVIEW software.

ASSOCIATED CONTENT

Supporting Information. (text)

Figure S1: TEM of AgNW/AlN, sample photo, bare AlN optical transmittance and optical band gap, physical properties of AgNW/AlN

Figure S2: XRR spectra and data fitting for AlN coatings

Figure S3: XPS spectra and analysis for as-deposited AgNW/AlN

Figure S4: XPS spectra of Ag3d before and after accelerated environmental stress for bare and AgNW/AlN

Figure S5: SEM images after the micro-scratch tests for bare and AgNW/AlN

Figure S6: SEM images and XPS spectra after thermal ramp and plateau for bare and AgNW/AlN

Figure S7: TEM as-dep for AgNW/Al_2O_3, optical transmittance spectra comparison between AlN and Al_2O_3 coated AgNW networks, bare Al_2O_3 optical transmittance and optical band gap

Figure S8: SEM after thermal ramp for AgNW/Al_2O_3

Table S1: Electrical properties before and after accelerated environmental stress

Table S2: Electrical resistance after thermal stress, ramp and plateau, experiments

Table S3: Physical properties of bare and AgNW/Al_2O_3

Supporting Information. (video)

Movie S1: IR imaging *in situ* during voltage ramp depicted in Figure 3a-Bare

Movie S2: IR imaging *in situ* during voltage ramp depicted in Figure 3a- C19.6

Movie S3: IR imaging *in situ* during voltage ramp depicted in Figure 4a-AlN-6.2

Movie S4: IR imaging *in situ* during voltage ramp depicted in Figure 4a-AlN-8.8

Movie S5: IR imaging *in situ* during voltage ramp depicted in Figure 4a-AlN-13.3

Movie S6: IR imaging *in situ* during voltage ramp depicted in Figure 4a-Al_2O_3-6.6

Movie S7: IR imaging *in situ* during voltage ramp depicted in Figure 4a-Al_2O_3-9.5

Movie S8: IR imaging *in situ* during voltage ramp depicted in Figure 4a- Al_2O_3-13.0

AUTHOR INFORMATION

Corresponding Authors

*E-mail: david.munoz-rojas@grenoble-inp.fr

*E-mail: elisabeth.blanquet@simap.grenoble-inp.fr

Authors ORCID

Dorina T. Papanastasiou https://orcid.org/0000-0001-8471-8789

Arnaud Mantoux https://orcid.org/0000-0001-9043-7465

Alexandre Crisci https://orcid.org/0000-0002-1812-9537

Hugo Ribeiro https://orcid.org/0009-0004-9289-8096

Abderrahime Sekkat https://orcid.org/0000-0002-8008-3357

Hervé Roussel https://orcid.org/0000-0001-6110-5760

Matthieu Weber https://orcid.org/0000-0003-2490-6168

Laetitia Rapenne https://orcid.org/0000-0003-1896-2315

Carmen Jiménez https://orcid.org/0000-0002-9601-1825

Marc Fivel https://orcid.org/0000-0002-0393-2191

Daniel Bellet https://orcid.org/0000-0002-9929-3696

Elisabeth Blanquet https://orcid.org/0000-0001-6467-9110

David Muñoz-Rojas https://orcid.org/0000-0003-1234-0814

Author Contributions

The manuscript was written through contributions of all authors. All authors have given approval to the final version of the manuscript.

Notes

The authors declare no competing financial interest.

ACKNOWLEDGMENT

This study was performed within the framework of the Centre of Excellence of Multifunctional Architectured Materials (CEMAM) n°ANR-10-LABX-44-01. Agence Nationale de la Recherche (ANR) is acknowledged for financial support under contracts ANR-18-CE09-0040 (MEANING)

and ANR-18-CE09-0036 (PANASSE). D.T.P. acknowledges Japan Society for the Promotion of Science (JSPS) for Postdoctoral Fellowship for Research in Japan (Standard).

REFERENCES

(1) Nguyen, V. H.; Papanastasiou, D. T.; Resende, J.; Bardet, L.; Sannicolo, T.; Jiménez, C.; Muñoz-Rojas, D.; Nguyen, N. D.; Bellet, D. Advances in Flexible Metallic Transparent Electrodes. *Small* **2022**, 2106006. https://doi.org/10.1002/smll.202106006.

(2) Papanastasiou, D. T.; Schultheiss, A.; Muñoz-Rojas, D.; Celle, C.; Carella, A.; Simonato, J.-P.; Bellet, D. Transparent Heaters: A Review. *Adv. Funct. Mater.* **2020**, *30* (21), 1910225. https://doi.org/10.1002/adfm.201910225.

(3) Hofmann, A. I.; Cloutet, E.; Hadziioannou, G. Materials for Transparent Electrodes: From Metal Oxides to Organic Alternatives. *Adv. Electron. Mater.* **2018**, *4* (10), 1700412. https://doi.org/10.1002/aelm.201700412.

(4) Ouyang, J. Application of Intrinsically Conducting Polymers in Flexible Electronics. *SmartMat* **2021**, *2* (3), 263–285. https://doi.org/10.1002/smm2.1059.

(5) Xu, Y.; Liu, J. Graphene as Transparent Electrodes: Fabrication and New Emerging Applications. *Small* **2016**, *12* (11), 1400–1419. https://doi.org/10.1002/smll.201502988.

(6) Sannicolo, T.; Lagrange, M.; Cabos, A.; Celle, C.; Simonato, J.-P.; Bellet, D. Metallic Nanowire-Based Transparent Electrodes for Next Generation Flexible Devices: A Review. *Small* **2016**, *12* (44), 6052–6075. https://doi.org/10.1002/smll.201602581.

(7) Huang, Q.; Zhu, Y. Patterning of Metal Nanowire Networks: Methods and Applications. *ACS Appl. Mater. Interfaces* **2021**, *13* (51), 60736–60762. https://doi.org/10.1021/acsami.1c14816.

(8) Choi, C.; Schlenker, E.; Ha, H.; Cheong, J. Y.; Hwang, B. Versatile Applications of Silver Nanowire-Based Electrodes and Their Impacts. *Micromachines* **2023**, *14* (3), 562. https://doi.org/10.3390/mi14030562.

(9) Yu, K.; He, T. Silver-Nanowire-Based Elastic Conductors: Preparation Processes and Substrate Adhesion. *Polymers* **2023**, *15* (6), 1545. https://doi.org/10.3390/polym15061545.

(10) Ding, Y.; Cui, Y.; Liu, X.; Liu, G.; Shan, F. Welded Silver Nanowire Networks as High-Performance Transparent Conductive Electrodes: Welding Techniques and Device Applications. *Appl. Mater. Today* **2020**, *20*, 100634. https://doi.org/10.1016/j.apmt.2020.100634.

(11) Guan, P.; Zhu, R.; Zhu, Y.; Chen, F.; Wan, T.; Xu, Z.; Joshi, R.; Han, Z.; Hu, L.; Wu, T.; Lu, Y.; Chu, D. Performance Degradation and Mitigation Strategies of Silver Nanowire Networks: A Review. *Crit. Rev. Solid State Mater. Sci.* **2022**, *47* (3), 435–459. https://doi.org/10.1080/10408436.2021.1941753.

(12) Patil, J. J.; Chae, W. H.; Trebach, A.; Carter, K.; Lee, E.; Sannicolo, T.; Grossman, J. C. Failing Forward: Stability of Transparent Electrodes Based on Metal Nanowire Networks. *Adv. Mater.* **2021**, *33* (5), 2004356. https://doi.org/10.1002/adma.202004356.

(13) Resende, J.; Papanastasiou, D. T.; Moritz, D. C.; Fontanals, N.; Jiménez, C.; Muñoz-Rojas, D.; Bellet, D. Time of Failure of Metallic Nanowire Networks under Coupled Electrical and Thermal Stress: Implications for Transparent Electrodes Lifetime. *ACS Appl. Nano Mater.* **2022**, *5* (2), 2102. https://doi.org/10.1021/acsanm.1c03821.

(14) Bang, J.; Coskun, S.; Pyun, K. R.; Doganay, D.; Tunca, S.; Koylan, S.; Kim, D.; Unalan, H. E.; Ko, S. H. Advances in Protective Layer-Coating on Metal Nanowires with Enhanced Stability and Their Applications. *Appl. Mater. Today* **2021**, *22*, 100909. https://doi.org/10.1016/j.apmt.2020.100909.

(15) Liu, W.; Hu, Y.; Chen, Y.; Hu, Z.; Zhou, K.; Min, Z.; Liu, H.; Zhan, L.; Dai, Y. Improvement of Electrical Properties of Silver Nanowires Transparent Conductive by Metal Oxide Nanoparticles Modification. *Coatings* **2022**, *12* (12), 1816. https://doi.org/10.3390/coatings12121816.

(16) Zhang, X.; Shan, J.; Liu, C.; Li, Z.; Guo, X.; Zhao, X.; Yang, H. High Corrosion-Resistant Silver Nanowire/Poly(3,4-Ethylene Dioxythiophene)/Poly (Styrene Sulfonate)@nickel Electrode for Transparent Electromagnetic Shielding Film. *J. Materiomics* **2022**, *8* (6), 1191–1198. https://doi.org/10.1016/j.jmat.2022.05.008.

(17) Azani, M.-R.; Hassanpour, A.; Torres, T. Benefits, Problems, and Solutions of Silver Nanowire Transparent Conductive Electrodes in Indium Tin Oxide (ITO)-Free Flexible Solar Cells. *Adv. Energy Mater.* **2020**, *10* (48), 2002536. https://doi.org/10.1002/aenm.202002536.

(18) Wang, K.; Jin, Y.; Xiao, F. Long-Term Electrically Stable Silver Nanowire Composite Transparent Electrode under High Current Density. *J. Mater. Sci. Mater. Electron.* **2021**. https://doi.org/10.1007/s10854-021-06386-4.

(19) Patil, J. J.; Reese, M. L.; Lee, E.; Grossman, J. C. Oxynitride-Encapsulated Silver Nanowire Transparent Electrode with Enhanced Thermal, Electrical, and Chemical Stability. *ACS Appl. Mater. Interfaces* **2022**, *14* (3), 4423–4433. https://doi.org/10.1021/acsami.1c20521.

(20) Bardet, L.; Papanastasiou, D. T.; Crivello, C.; Akbari, M.; Resende, J.; Sekkat, A.; Sanchez-Velasquez, C.; Rapenne, L.; Jiménez, C.; Muñoz-Rojas, D.; Denneulin, A.; Bellet, D. Silver Nanowire Networks: Ways to Enhance Their Physical Properties and Stability. *Nanomaterials* **2021**, *11* (11), 2785. https://doi.org/10.3390/nano11112785.

(21) Liu, G.; Wang, J.; Ge, Y.; Wang, Y.; Lu, S.; Zhao, Y.; Tang, Y.; Soomro, A. M.; Hong, Q.; Yang, X.; Xu, F.; Li, S.; Chen, L.-J.; Cai, D.; Kang, J. Cu Nanowires Passivated with Hexagonal Boron Nitride: An Ultrastable, Selectively Transparent Conductor. *ACS Nano* **2020**, *14* (6), 6761–6773. https://doi.org/10.1021/acsnano.0c00109.

(22) *Properties of Advanced Semiconductor Materials: GaN, AlN, InN, BN, SiC, SiGe*; Levinshteĭn, M. E., Rumyantsev, S. L., Shur, M., Eds.; Wiley: New York, 2001.

(23) Tian, L.; Ponton, S.; Benz, M.; Crisci, A.; Reboud, R.; Giusti, G.; Volpi, F.; Rapenne, L.; Vallée, C.; Pons, M.; Mantoux, A.; Jiménez, C.; Blanquet, E. Aluminum Nitride Thin Films Deposited by Hydrogen Plasma Enhanced and Thermal Atomic Layer Deposition. *Surf. Coat. Technol.* **2018**, *347*, 181–190. https://doi.org/10.1016/j.surfcoat.2018.04.031.

(24) Österlund, E.; Kinnunen, J.; Rontu, V.; Torkkeli, A.; Paulasto-Kröckel, M. Mechanical Properties and Reliability of Aluminum Nitride Thin Films. *J. Alloys Compd.* **2019**, *772*, 306–313. https://doi.org/10.1016/j.jallcom.2018.09.062.

(25) Huang, Z.; Li, S.; Guo, H.; Huang, C.; Bian, Y.; Gong, Y.; Huang, J.; Zeng, Q. Multi-Scale GO/CNT/AlN Nanocomposites for High-Performance Flexible Electrothermal Film Heaters. *J. Mater. Chem. C* **2023**, 10.1039.D3TC01265D. https://doi.org/10.1039/D3TC01265D.

(26) Lee, W.; Kim, J. Highly Thermal Conductive and Electrical Insulating Epoxy Composites with a Three-Dimensional Filler Network by Sintering Silver Nanowires on Aluminum Nitride Surface. *Polymers* **2021**, *13* (5), 694. https://doi.org/10.3390/polym13050694.

(27) Shen, J.; Roozeboom, F.; Mameli, A. Atmospheric-Pressure Plasma-Enhanced Spatial Atomic Layer Deposition of Silicon Nitride at Low Temperature. *At. Layer Depos.* **2023**, *1*, 1–11. https://doi.org/10.3897/aldj.1.101651.
(28) De La Huerta, C. A. M.; Nguyen, V. H.; Sekkat, A.; Crivello, C.; Toldra-Reig, F.; Veiga, P. B.; Quessada, S.; Jimenez, C.; Muñoz-Rojas, D. Gas-Phase 3D Printing of Functional Materials. *Adv. Mater. Technol.* **2020**, *5* (12), 2000657. https://doi.org/10.1002/admt.202000657.
(29) Bardet, L.; Akbari, M.; Crivello, C.; Rapenne, L.; Weber, M.; Nguyen, V. H.; Jiménez, C.; Muñoz-Rojas, D.; Denneulin, A.; Bellet, D. SnO_2 -Coated Silver Nanowire Networks as a Physical Model Describing Their Reversible Domain under Electrical Stress for Stable Transparent Electrode Applications. *ACS Appl. Nano Mater.* **2023**, *6* (16), 15234–15246. https://doi.org/10.1021/acsanm.3c03008.
(30) Bardet, L.; Roussel, H.; Saroglia, S.; Akbari, M.; Muñoz-Rojas, D.; Jiménez, C.; Denneulin, A.; Bellet, D. Exploring the Degradation of Silver Nanowire Networks under Thermal Stress by Coupling *in Situ* X-Ray Diffraction and Electrical Resistance Measurements. *Nanoscale* **2024**, *16* (2), 564–579. https://doi.org/10.1039/D3NR02663A.
(31) *Handbook of X-Ray Photoelectron Spectroscopy: A Reference Book of Standard Spectra for Identification and Interpretation of XPS Data*; Moulder, J. F., Stickle, W. F., Sobol, P. E., Bomben, K. D., Chastain, J., King Jr., R. C., Physical Electronics, Incorporation, Eds.; Physical Electronics: Eden Prairie, Minn., 1995.
(32) Martin, P.; Netterfield, R.; Kinder, T.; Bendavid, A. Optical Properties and Stress of Ion-Assisted Aluminum Nitride Thin Films. *Appl. Opt.* **1992**, *31* (31), 6734. https://doi.org/10.1364/AO.31.006734.
(33) Li, X.; Gao, H.; Murphy, C. J.; Caswell, K. K. Nanoindentation of Silver Nanowires. *Nano Lett.* **2003**, *3* (11), 1495–1498. https://doi.org/10.1021/nl034525b.
(34) Lucas, M.; Leach, A. M.; McDowell, M. T.; Hunyadi, S. E.; Gall, K.; Murphy, C. J.; Riedo, E. Plastic Deformation of Pentagonal Silver Nanowires: Comparison between AFM Nanoindentation and Atomistic Simulations. *Phys. Rev. B* **2008**, *77* (24), 245420. https://doi.org/10.1103/PhysRevB.77.245420.
(35) Papanastasiou, D. T.; Carlos, E.; Muñoz-Rojas, D.; Jiménez, C.; Pimentel, A.; Fortunato, E.; Martins, R.; Bellet, D. Fully Solution-Based AgNW/AlO_x Nanocomposites for Stable Transparent Heaters. *ACS Appl. Electron. Mater.* **2022**, *4* (12), 5816–5824. https://doi.org/10.1021/acsaelm.2c01007.
(36) Khan, A.; Nguyen, V. H.; Muñoz-Rojas, D.; Aghazadehchors, S.; Jiménez, C.; Nguyen, N. D.; Bellet, D. Stability Enhancement of Silver Nanowire Networks with Conformal ZnO Coatings Deposited by Atmospheric Pressure Spatial Atomic Layer Deposition. *ACS Appl. Mater. Interfaces* **2018**, *10* (22), 19208–19217. https://doi.org/10.1021/acsami.8b03079.
(37) Charvin, N.; Resende, J.; Papanastasiou, D. T.; Muñoz-Rojas, D.; Jiménez, C.; Nourdine, A.; Bellet, D.; Flandin, L. Dynamic Degradation of Metallic Nanowire Networks under Electrical Stress: A Comparison between Experiments and Simulations. *Nanoscale Adv.* **2021**, *3* (3), 675–681. https://doi.org/10.1039/D0NA00895H.
(38) Hoque, M. S. B.; Koh, Y. R.; Braun, J. L.; Mamun, A.; Liu, Z.; Huynh, K.; Liao, M. E.; Hussain, K.; Cheng, Z.; Hoglund, E. R.; Olson, D. H.; Tomko, J. A.; Aryana, K.; Galib, R.; Gaskins, J. T.; Elahi, M. M. M.; Leseman, Z. C.; Howe, J. M.; Luo, T.; Graham, S.; Goorsky, M. S.; Khan, A.; Hopkins, P. E. High In-Plane Thermal Conductivity of

Aluminum Nitride Thin Films. *ACS Nano* **2021**, *15* (6), 9588–9599. https://doi.org/10.1021/acsnano.0c09915.

(39) Li, J.; Tao, Y.; Chen, S.; Li, H.; Chen, P.; Wei, M.; Wang, H.; Li, K.; Mazzeo, M.; Duan, Y. A Flexible Plasma-Treated Silver-Nanowire Electrode for Organic Light-Emitting Devices. *Sci. Rep.* **2017**, *7* (1), 16468. https://doi.org/10.1038/s41598-017-16721-7.

(40) Liu, J.; Ge, Y.; Zhang, D.; Han, M.; Li, M.; Zhang, M.; Duan, X.; Yang, Z.; Hu, J. Plasma Cleaning and Self-Limited Welding of Silver Nanowire Films for Flexible Transparent Conductors. *ACS Appl. Nano Mater.* **2021**, *4* (2), 1664–1671. https://doi.org/10.1021/acsanm.0c03137.

(41) Aghazadehchors, S.; Nguyen, V. H.; Muñoz-Rojas, D.; Jiménez, C.; Rapenne, L.; Nguyen, N. D.; Bellet, D. Versatility of Bilayer Metal Oxide Coatings on Silver Nanowire Networks for Enhanced Stability with Minimal Transparency Loss. *Nanoscale* **2019**, *11* (42), 19969–19979. https://doi.org/10.1039/C9NR05658K.

(42) Lee, J.-H.; Choi, T.-Y.; Cheon, H.-S.; Youn, H.-Y.; Lee, G.-W.; Lee, S.-N.; Kim, H.-K. Conformal and Transparent Al2O3 Passivation Coating via Atomic Layer Deposition for High Aspect Ratio Ag Network Electrodes. *Metals* **2023**, *13* (3), 528. https://doi.org/10.3390/met13030528.

(43) Mayousse, C.; Celle, C.; Moreau, E.; Mainguet, J.-F.; Carella, A.; Simonato, J.-P. Improvements in Purification of Silver Nanowires by Decantation and Fabrication of Flexible Transparent Electrodes. Application to Capacitive Touch Sensors. *Nanotechnology* **2013**, *24* (21), 215501. https://doi.org/10.1088/0957-4484/24/21/215501.

(44) Nguyen, V. H.; Resende, J.; Papanastasiou, D. T.; Fontanals, N.; Jiménez, C.; Muñoz-Rojas, D.; Bellet, D. Low-Cost Fabrication of Flexible Transparent Electrodes Based on Al Doped ZnO and Silver Nanowire Nanocomposites: Impact of the Network Density. *Nanoscale* **2019**, *11* (25), 12097–12107. https://doi.org/10.1039/C9NR02664A.

(45) Muñoz-Rojas, D.; Maindron, T.; Esteve, A.; Piallat, F.; Kools, J. C. S.; Decams, J.-M. Speeding up the Unique Assets of Atomic Layer Deposition. *Mater. Today Chem.* **2019**, *12*, 96–120. https://doi.org/10.1016/j.mtchem.2018.11.013.

(46) Schultheiss, A.; Sekkat, A.; Nguyen, V. H.; Carella, A.; Benayad, A.; Revaux, A.; Demadrille, R.; Muñoz-Rojas, D.; Simonato, J.-P. High Performance Encapsulation of Transparent Conductive Polymers by Spatial Atomic Layer Deposition. *Synth. Met.* **2022**, *284*, 116995. https://doi.org/10.1016/j.synthmet.2021.116995.

(47) Sannicolo, T.; Charvin, N.; Flandin, L.; Kraus, S.; Papanastasiou, D. T.; Celle, C.; Simonato, J.-P.; Muñoz-Rojas, D.; Jiménez, C.; Bellet, D. Electrical Mapping of Silver Nanowire Networks: A Versatile Tool for Imaging Network Homogeneity and Degradation Dynamics during Failure. *ACS Nano* **2018**, *12* (5), 4648–4659. https://doi.org/10.1021/acsnano.8b01242.

(48) Papanastasiou, D. T.; Sekkat, A.; Nguyen, V. H.; Jiménez, C.; Muñoz-Rojas, D.; Bruckert, F.; Bellet, D. Stable Flexible Transparent Electrodes for Localized Heating of Lab-on-a-Chip Devices. *Adv. Mater. Technol.* **2023**, *8* (1), 2200563. https://doi.org/10.1002/admt.202200563.

(49) Hanauer, S.; Celle, C.; Crivello, C.; Szambolics, H.; Muñoz-Rojas, D.; Bellet, D.; Simonato, J.-P. Transparent and Mechanically Resistant Silver-Nanowire-Based Low-Emissivity Coatings. *ACS Appl. Mater. Interfaces* **2021**, *13* (18), 21971. https://doi.org/10.1021/acsami.1c02689.

BRIEFS Ultra-thin aluminum nitride coatings were deposited for the first time on top of silver nanowire networks, leading to transparent electrodes with remarkable robustness and stability.

SYNOPSIS Table of Contents Graphic